Experimental evidence for dynamic friction on rock fractures from frequency-dependent nonlinear hysteresis and harmonic generation

Seth Saltiel

Brian P. Bonner

Tushar Mittal

Brent Delbridge

Jonathan B. Ajo-Franklin
First published: 29 June 2017

https://doi.org/10.1002/2017JB014219
UC-eLinks

Abstract

Frictional properties affect the propagation of high-amplitude seismic waves across rock fractures and faults. Laboratory evidence suggests that these properties can be measured in active seismic surveys, potentially offering a route to characterizing friction in situ. We present experimental results from a subresonance torsional modulus and attenuation apparatus that utilizes micron-scale sinusoidal oscillations to probe the nonlinear stress-strain relation at a range of strain amplitudes and rates. Nonlinear effects are further quantified using harmonic distortion; however, time series data best illuminate underlying physical processes. The low-frequency stress-strain hysteretic loops show stiffening at the sinusoid's static ends, but stiffening is reduced above a threshold frequency. This shape is determined by harmonic generation in the strain; the stress signal has no harmonics, confirming that the fractured sample is the source of the nonlinearity. These qualitative observations suggest the presence of rate-dependent friction and are consistent between fractures in three different rock types. We propose that static friction at the low strain rate part of the cycle, when given sufficient “healing” time at low oscillation frequencies, causes this stiffening cusp shape in the hysteresis loop. While rate-and-state friction is commonly used to represent dynamic friction, it cannot capture static friction or negative slip velocities. So we implement another dynamic friction model, based on the work of Dahl, which

describes this process and produces similar results. Since the two models have a similar form, parameterizations of field data could constraint fault model inputs, such as specific location velocity strengthening or weakening properties.

1 Introduction

Geophysical measurements of open fractures and faults in the subsurface can potentially provide constraints on the mechanical state of fractures [e.g., *Pyrake-Nolte*, 1996] including parameters such as stress state, frictional properties, and fluid occupancy. Time-lapse seismic measurements can be used to monitor these processes and their changes during reservoir manipulations, such as the direct effect of injectants (e.g., supercritical CO_2) [e.g., *Daley et al.*, 2007], or other natural stress changes [e.g., *Niu et al.*, 2008]. For example, frictional properties and processes could be measured by inducing partial slip on fracture faces with repeatable high-amplitude shear waves [*Saltiel et al.*, 2017b]. The properties of transmitted waves, including their amplitude and frequency dependences, could constrain the frictional properties of the subsurface interface. In order to interpret field measurements, the sensitivity and parametric form of these frictional processes must be determined with laboratory-scale experiments.

The frictional behavior of rocks is of fundamental relevance to a range of seismic processes, from the earthquake cycle to triggered and induced seismicity. Most earthquakes are shear displacements generated by unstable stick slip in which the fault's interface transitions from static to dynamic friction [*Scholz*, 2002]. Friction has been shown to increase with the logarithm of time spent under static conditions, a process referred to as healing [e.g., *Li et al.*, 2011]. This effect is captured by slide-hold-slide lab experiments, while most other experiments focus on constant load point velocities or velocity steps [e.g., *Marone*, 1998]. Only limited laboratory work has explored periodic shear loading [*Savage and Marone*, 2007] or transient dynamic stresses [*Savage and Marone*, 2008; *van der Elst and Savage*, 2015; *Johnson et al.*, 2016]. These experiments probe slide-slip behavior, where the periodic loading is superimposed on top of a constant positive slip velocity, so static friction or reverse slip is never reached. These studies focused on understanding dynamically triggered earthquakes [e.g., *Hill et al.*, 1991]. Earthquake triggering could provide a probe of the stress state and frictional properties of the fault [*Voisin*, 2001; *Voisin*, 2002]. By identifying the processes that govern dynamic triggering of frictional slip instabilities in laboratory experiments, field observations of triggered events can provide information on the in situ critical shear stress state proceeding earthquake failure [e.g., *Brodsky and van der Elst*, 2014; *van der Elst et al.*, 2016; *Delorey et al.*, 2016; *Johnson et al.*, 2016]. In laboratory experiments, triggering was found to have a complicated dependence on the frequency of the perturbation; hence, fault friction itself has a complex frequency

dependence, exhibiting a range of regimes [e.g., *Savage and Marone*, 2007; *Savage and Marone*, 2008; *van der Elst and Savage*, 2015]. This study focuses on illuminating the frequency dependence of friction experimentally. In order to help interpret and motivate further field measurements, we measure and model the response of a mated rock fracture experiencing forced oscillations through static, zero strain rate, and friction conditions.

In contrast to interface friction, the frequency dependence of elastic moduli, or dispersion, has been extensively studied because of its direct connection to the attenuation of seismic waves in anelastic medium [e.g., *Mavko et al.*, 2009]. The frequency dependence of parameters governing seismic wave propagation has been shown in the laboratory for a number of hypothesized attenuation processes (e.g., scattering, wave-induced fluid flow, and friction). Most recent studies focus on the dispersive behavior induced by fluid saturation [e.g., *Tisato et al.*, 2014; *Subramaniyan et al.*, 2014; *Spencer and Shine*, 2016] with the hope that attenuation measurements in the field could be used to locate, identify, and quantify fluids as well as matrix permeability in the subsurface [*Pride et al.*, 2003]. The frequency dependence caused by fluids is dependent on the mobility of fluid in the pore space, so measuring the attenuation and frequency dispersion should give information about the fluid viscosity and rock permeability [e.g., *Spencer*, 1981; *Batzle et al.*, 2006; *Spencer and Shine*, 2016].

The Kramers-Kronig relations insure that any energy dissipation, or hysteresis, causes frequency dependence in linear anelastic materials [e.g., *O'Donnell et al.*, 1981]. Thus, attenuation and frequency dispersion are expected for cases of hysteretic cyclical loading and unloading on crack interfaces [*Walsh*, 1966; *David et al.*, 2012]. Frictional attenuation has been studied experimentally and theoretically for strains above about 10^{-6} [e.g., *Gordon and Davis*, 1968; *McKavanagh and Stacey*, 1974; *Cooper*, 1979; *Mavko*, 1979]. Crack friction was typically ignored as a dominant form of attenuation, because most seismic waves away from the source have strain below 10^{-6}, which will induce smaller than interatomic spacing scale (~10^{-8} cm) displacement on cracks of length less than 10^{-2} cm, a rough upper bound for the majority of crack lengths in intact rock [*Savage*, 1969; *Winkler et al.*, 1979]. The impact of frictional attenuation must be revisited when the size of fractures is larger or for higher-amplitude seismic waves. Under these conditions, friction on fracture faces may be detectable seismically, thus providing a way to infer important, interrelated fracture properties—such as displacement, fracture density, asperity contact area, aperture, stiffness, or friction coefficient—in the field [*Pyrake-Nolte and Morris*, 2000; *Pyrake-Nolte and Nolte*, 2016]. In this case the frequency dispersion and attenuation could be tied to the rate-dependent frictional properties of the interface.

Strain-dependent modulus changes have also been observed at strains greater than about 10^{-6} [*Guyer and Johnson*, 2009]. These changes in modulus have been shown to recover with log time, referred to as slow dynamics [e.g., *Smith and TenCate*, 2000; *Lebedev and Ostrovsky*, 2014; *Snieder et al.*, 2017]. Nonelliptical stress-strain hysteresis loops, called "cusps" because they sharpen to a point at each end, are another sign of this nonlinearity observed for rocks under higher strain levels [*Gordon and Davis*, 1968; *McKavanagh and Stacey*, 1974]. This nonlinear hysteresis, with end-point memory, has been described using a Preisach-Mayergoyz (PM) model space of hysteretic elements that open and close at different stresses [*Guyer et al.*, 1995; *Guyer et al.*, 1997]. Nonclassical nonlinearity, which cannot be described by traditional theories of nonlinear elasticity [e.g., *Landau and Lifshitz*, 1986; *Pasqualini et al.*, 2007], has been observed in a range of microcracked, but intact, rock types [*Rivière et al.*, 2015] and wave types [*Remillieux et al.*, 2016]. The degree of nonlinearity reported in these studies is more modest than might be expected for a large fracture with no continuous material fully bridging the sample. Assuming that the physical mechanisms are similar, studying macroscopic fractures in the lab should allow evaluation of more subtle effects, such as frequency dependence, and characterize the interface geometry that determines the frictional behavior.

Few measurements have focused on the frequency (strain rate) dependence of nonclassical nonlinearity. Frequency dependency has been suggested in the difference between quasi-static and three wave mixing dynamic measurements of nonlinear parameters on sandstones and a limestone [*D'Angelo et al.*, 2008]. In the Dynamic Acousto-Elastic Testing approach a lower frequency pump is used to induce nonlinearity, while a high-frequency probe detects the change in elastic constants with strain amplitude, and thus, the nonlinear elastic constants can be determined [*Rivière et al.*, 2013]. This method has been used on Berea sandstone to show that some constants are sensitive to the frequency of the pump signal between 0.2 and 250 Hz, while others are frequency independent, suggesting that at least two physical mechanisms are present in the nonlinearity [*Rivière et al.*, 2016a]. Further experiments demonstrated that some rocks have a preferential relaxation around 0.1 s–1 s, or 10 Hz–1 Hz, which was insensitive to the amplitude of the pump or moisture in the sample [*Rivière et al.*, 2016b]. A few models have been proposed to explain, or predict, frequency or rate-dependent nonlinearity [e.g., *Vakhnenko et al.*, 2005; *Gliozzi and Scalerandi*, 2014; *Pecorari*, 2015; *Favrie et al.*, 2015]. *Gusev and Tournat* [2005] added thermal induced transitions to a PM model space, referred to as Preisach-Arrhenius model, to explain a frequency as well as amplitude criterion for the onset of nonlinear elasticity. However, little research has focused on fully characterizing or understanding the rate dependence of potential physical mechanisms responsible for elastic nonlinearity in fractured

heterogeneous solids. This is necessary to fully understand the mechanisms responsible for the nonlinearity as well as the energy dissipation. Experiments are also needed to predict the sensitivity of various seismic methods to measure these processes in the field.

We have adapted a low-frequency (0.1–100 Hz) shear modulus and attenuation apparatus to explore the seismic signature of fractures and understand the mechanics of asperity contacts under low normal stresses and a range of shear strains. Our instrument is unique in its capacity to measure low-frequency seismic properties at low normal stresses, simulating “open” fractures in shallow or high fluid pressure reservoirs, which often dominate the permeability and may be the most likely source of induced seismicity. These are also the conditions where fractures initiate partial slip, with displacements at the micron scale. We focus on time series measurements of nonlinear elasticity and study the frequency dependence in hope of being able to interpret this signal to obtain more information from fractures in the field. Eventually, observing changes in the nonlinear metrics with injection of different fluids during stimulation could be used to identify the migration and efficacy of these injectants. Fitting the measurements with dynamic friction constitutive relations will also help constrain the general frictional behavior of rock fractures and larger-scale faults in the subsurface, providing valuable information about the potential for future seismicity.

2 Methods and Materials

2.1 Low-Frequency Torsional Apparatus and Analysis Techniques

We utilize a forced torsional oscillator to directly measure the shear stress and strain of cylindrical rock samples (9 mm diameter with various lengths). The apparatus (Figure 1) is a segmented torsional spring. One end is rigidly coupled to a magnetic driver, which sinusoidally twists the entire bar of the apparatus in series from a fixed point at the other end. Since all the components of the apparatus are assumed elastic on the time scales of interest, the torque (and shear stress) is transmitted evenly throughout the entire bar length and by measuring the amount and timing of the twist at various locations along this bar we can calculate the shear stress and strain directly, giving the modulus and attenuation of the sample under the given conditions. All of our experiments include a “pretwist” static load applied to the sample, oscillating the torque around that point. This allows oscillation without added hysteresis from going through the neutral point, so strain is always positive but strain rate oscillates between positive and negative values. The DC offset in stress and strain is subtracted from the reported time series stress and strain values to isolate the amplitude of the stress and strain oscillation, which determines the

modulus of the sample. We report the shear strain, and displacement, at the outside radius of the sample, since this is the maximum and contributes the most area, but in reality there is a gradient in strain proportional to distance from the center of the sample. A detailed description of the apparatus and error analysis, including that due to long-term drift (temperature, humidity, fatigue…), are given in *Saltiel et al.* [2017a].

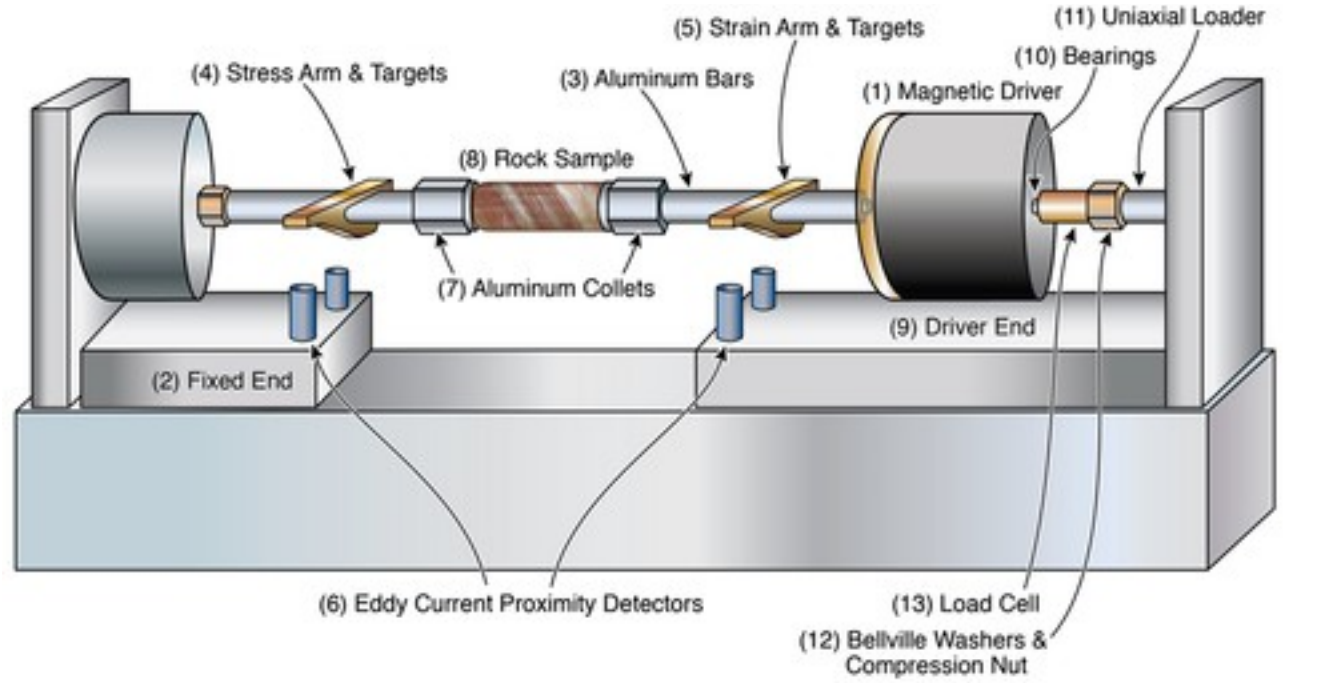

Figure 1

Open in figure viewerPowerPoint

Schematic diagram and photograph of instrument, with parts labeled as in text: (1) Magnetic driver, half of the black magnetic shielding is removed in photograph. (2) End of apparatus held fixed. (3) Aluminum bars that transmit stress; fixed end bar is hollow to amplify the torque signal. (4) Arm and targets for measuring twist on fixed side of sample, calibrated to an imposed static shear stress. (5) Arm and targets for measuring twist on driver side of sample, calibrated to shear strain. (6) Eddy current proximity detectors that measure displacement, and thus twist, of the two sets of arms and targets. (7) Aluminum collets that hold sample. (8) Fractured rock sample, aluminum in photograph. (9) Driver end that is free to twist. (10) Hardened ball bearings that limit nontorsional motion in the driver and insure purely uniaxial force from loader. (11)

Uniaxial loader that applies normal stress to fractures. (12) Bellville washers supply compression as the nut is tightened. (13) Load cell measures applied uniaxial stress with a calibrated strain gauge. Figure and description from *Saltiel et al.*[2017a].

We follow a specific protocol to measure each sample, before and after tensile fracturing, under a range of strain amplitudes, frequencies, and normal stresses. First, the intact sample is measured without uniaxial stress at 1 Hz, gradually increasing strain amplitude from about 10^{-6} to 5×10^{-5} over 1000 measurements. This is repeated for 2, 4, 8, 16, 32, and 64 Hz to explore the sample's frequency dispersion. The protocol is then repeated with increasing applied uniaxial stresses (up to about 15 MPa). The static load is changed directly to the next value, but the DC shear stress is removed while the new uniaxial load is set. The sample is then fractured using the method described below, and measured at the same uniaxial stress conditions, this time starting at the highest normal stresses and slowly decreasing normal stress until the fracture slips completely and it can no longer be measured with our method. Due to the large amount of data in the time series of thousands of oscillations, these experiments are analyzed using a Fourier transform of the stress and strain signals, only retaining the response at the forcing frequency, the fundamental mode. This assumes that the material is relatively linear (negligible harmonic generation). To study the nonlinear and dynamic response we record the entire low-frequency time series oscillations for each sample only at their lowest measurable normal stresses and highest shear amplitudes, where slip and frictional effects are enhanced. Graphing the stress and strain oscillations against each other provides stress-strain hysteresis loops. This time series approach provides more information about the strain rate dependence and allows detailed analysis of relevant frictional processes.

For perfectly linear anelastic materials, hysteresis is caused by a phase delay between the stress and the strain; the resulting hysteresis loop is an ellipse, the area of which is a measure of the energy dissipated, or the attenuation [*Zener*, 1948]. These materials would have stress and strain signals only at the driving frequency, or fundamental, since any harmonic generation of a nonlinear material will cause distortion in the shape of the hysteresis loop [*Guyer and Johnson*, 2009]. In this way, the harmonic distortion and hysteresis shape are directly related to each other and the nonlinearity of the material. Harmonic distortion in electronics, as well as acoustics, is commonly measured by the total harmonic distortion (THD %) [*Ramirez*, 1985]; we calculate it from the square root of the power of the first four harmonics over the square root of the power in the fundamental.

Further features make our instrument particularly well suited to studying nonlinearity in fractured rocks. First, the uniaxial stress assembly (part (11) in Figure 1) provides normal stress to close-up fractures and slowly open them with decreasing confinement. This can simulate

important processes in fractured reservoirs such as pore pressure (and thus effective stress) changes from injection or production. As mentioned previously, our system is capable of measurements at very low normal stress magnitudes, levels which are inherently difficult for other instruments that rely on pressure, often minimums of ~10 MPa, to make contact with the sample [e.g., *Li et al.*, 2014]. The magnetic driver's range of shear stresses also allows measurement under higher strains where nonlinearity is more pronounced and frictional sliding initiates on fracture surfaces. The driver can also be controlled with high precision, allowing us to bring the surfaces just to the brink of fully slipping (e.g., partial slip), while maintaining relatively small displacements. In this way, we can use the driver to induce slip or even propagate new fractures, while probing the response throughout the process. The apparatus can also be used to explore fatigue damage, by measuring how the response changes over millions of cycles.

2.2 Sample Description and Surface Characterization

We measured an artificially fractured dolomite core from the Duperow formation, a carbon sequestration target in north-central Montana. A picture of the dolomite sample and surface characterization of its induced fracture face are shown in Figure 2. The sample was cored from a depth of 1017.3 m (3337.7 ft) in the Danielson well (API 811151). The sample was cored adjacent to plug 34B, which was measured to have a density of 2.716 g cm^{-3}, a porosity of 2.51%, and a permeability of 0.01 mD [*Spangler*, 2014]. The ultrasonic *P* and *S*wave velocities for the plug were measured at 5340 ± 160 m/s and 3300 ± 100 m/s, respectively [*Saltiel et al.*, 2017a]. The cores, in addition to preliminary surface seismic and well log data, suggest that the reservoir has relatively low matrix permeability but many healed and partially healed natural fracture sets. Preliminary modeling [*Zhou et al.*, 2013] indicates that the pressure change will be significant and likely generate the dominant alteration in seismic properties from the proposed large-scale supercritical CO_2 injection; existing open fractures should be most sensitive to these increases in pore pressure. By studying a tensile fractured reservoir core we estimate how seismic techniques can measure stress and frictional changes in similar field-scale fractures.

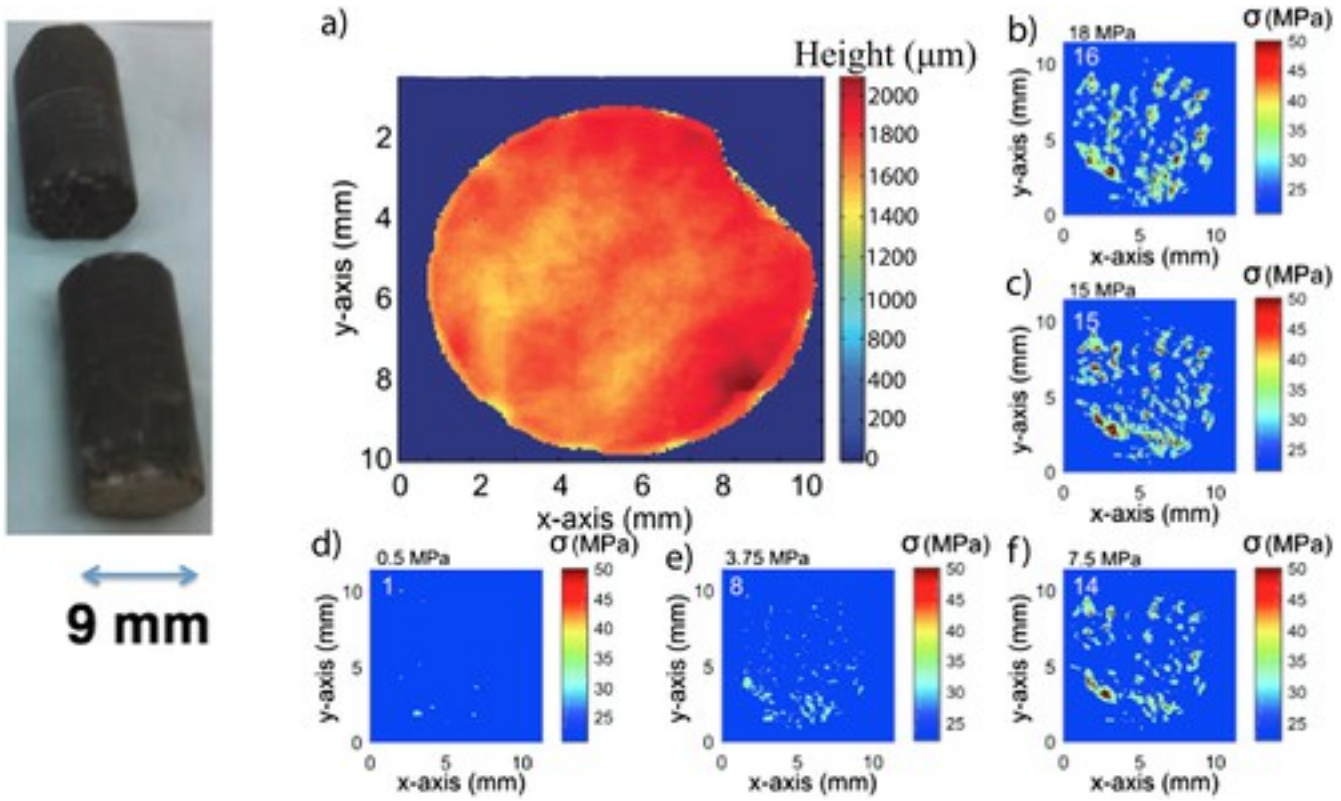

Figure 2

Open in figure viewerPowerPoint

Photograph and characterization of Duperow dolomite fracture surfaces show tensile fracturing created a relatively flat surface across the cylinder diameter. (a) Optical profilometry of surface topography. Local normal stress distribution from the calibrated pressure-sensitive film under normal stresses of (b) 18, (c) 15, (d) 0.5, (e) 3.75, and (f) 7.5 MPa. Figure modified from *Saltiel et al.* [2017a].

We also tested artificial tensile fractures in Montello granite and Blue Canyon Dome rhyolite samples to show that the general observed behavior is consistent with changes in rock type and surface geometry. The Montello is a competent, fine-grained granite, from a quarry in Wisconsin. It was selected because it has few microcracks and little stress dependence, so discriminating the effect of the throughgoing fracture from the rest of the intact rock is more straightforward. The Blue Canyon Dome rhyolite is a fine-grained, competent igneous rock from central New Mexico. Our sample was cored from an experimental field pilot site, utilized as a shallow analog for testing enhanced geothermal stimulation and relevant monitoring techniques [*Knox et al.*, 2016].

We employed a same custom-machined holder to generate a tensile fracture across the diameter of each sample. Twelve sharpened screws are positioned evenly around the holder and set into a groove carved around the circumference of the sample. As the screws are slowly tightened in a row around the diameter, they force open a tensile fracture that remains in the groove. This results in a well-mated tensile fracture, perpendicular to the diameter of the cylindrical sample,

with relatively smooth and low topography (Figure 2). As discussed in *Saltiel et al.* [2017a], we expect minimal process zone-related microfracturing. Optical profilometry and pressure sensitive film [*Selvadurai and Glaser*, 2015] were used to characterize the fracture surfaces; these techniques and analysis are described in *Saltiel et al.* [2017a]. The imaged contacts transmit shear stress as well as the measured normal stress across the fracture.

3 Results

3.1 Normal Stress and Strain Dependency in Fundamental Data

In *Saltiel et al.* [2017a], we measured the modulus and attenuation before and after fracturing under a range of uniaxial loads using 1000 measurements at the driving, fundamental, frequency (8 Hz). The error bars for each modulus and attenuation measurement are estimated from the error in linear fit of all 1000 stress-strain measurements and the standard deviation of all 1000 phase measurements. As can be seen in Figure 3a, the error bars at lowest normal stress, 0.375 MPa, are significantly larger than the other stress conditions, suggesting nonlinearity. In another publication [*Saltiel et al.*, 2017b], we focus on this lowest normal stress to explore the behavior of an open fracture where partial slip occurs. The attenuation and stress at the fundamental were recorded with strains from 5×10^{-6} to 5×10^{-5}, and the resulting stress-strain curves, with error bars in this case estimated from propagating the systematic error, fit with a single asperity partial slip model (Figure 3c), based on *Mindlin* [1949]. The model fit shows that partial slip on the outside of asperities can explain the observed softening, giving an effective asperity radius and friction coefficient; the model can also be extrapolated to fully slipping conditions, providing an estimate for the critical slip distance [*Saltiel et al.*, 2017b]. Figure 3b shows the average attenuation at each normal stress, where the error bars give the standard deviation of 1000 measurements; the intact dolomite sample is fairly attenuating, which masks the effect of the fracture. The lowest normal stress measurement has the highest attenuation, and it is strain-dependent (Figure 3d), as expected for frictional attenuation.

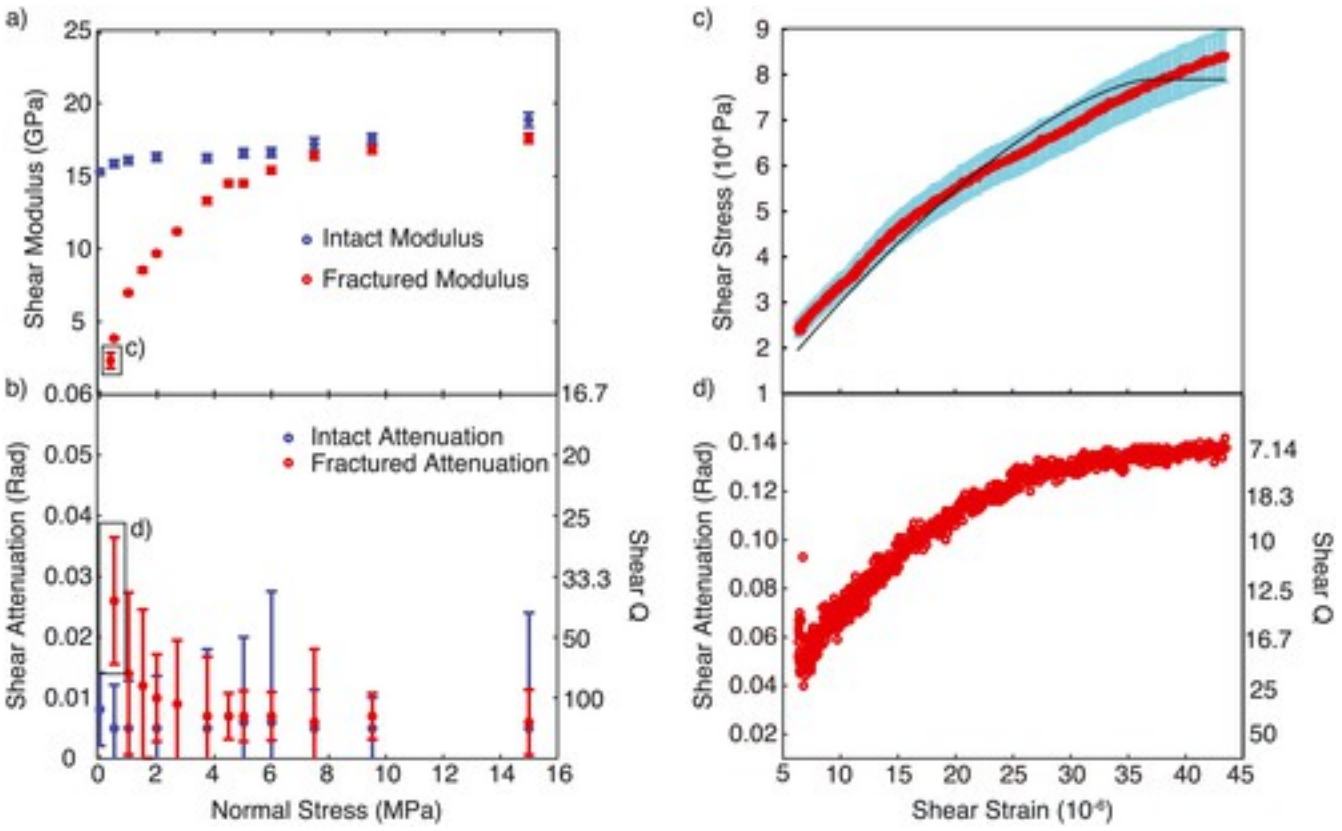

Figure 3

[Open in figure viewerPowerPoint]

Fundamental frequency (8 Hz) (a) modulus and (b) attenuation measurements for fractured and intact Duperow dolomite sample under a range of normal stresses. The error bars are estimated by the deviation in 1000 measurements over a range of amplitudes. The large error bars suggest nonlinear behavior under lowest normal stress (0.375 MPa). Measurement and analysis details are described in *Saltiel et al.* [2017a]. Strain-dependent (c) stress and (d) attenuation of lowest normal stress condition (0.375 MPa). Stress-strain curves are nonlinear and can be fit with a simple single asperity partial slip model, with error bars in this case are given by the systematic error. Attenuation is also strain-dependent, explained by frictional attenuation models. Measurement and analysis details are described in *Saltiel et al.* [2017b].

At the lowest normal stress (0.375 MPa), we also used a range of driving frequencies from 1 to 64 Hz. The intact dolomite shows normal dispersion, i.e., increasing modulus with frequency (Figure 4a). The fractured sample showed modulus decreasing with increasing frequency in the low-frequency range (1–4 Hz), and normal dispersion, as seen at higher normal stresses, resumes at higher frequencies (8–64 Hz) (Figure 4b). This inverse dispersion behavior is not expected for linear anelastic materials, where dispersion is directly related to dissipation [*Zener*, 1948], suggesting that the fracture is exhibiting nonlinear hysteresis. It also suggests that there may be a nonlinear process occurring at low frequencies (< ~8 Hz) in open fractures which is not present at higher frequencies (> ~8 Hz) or in closed fractures, or intact, microcracked rocks.

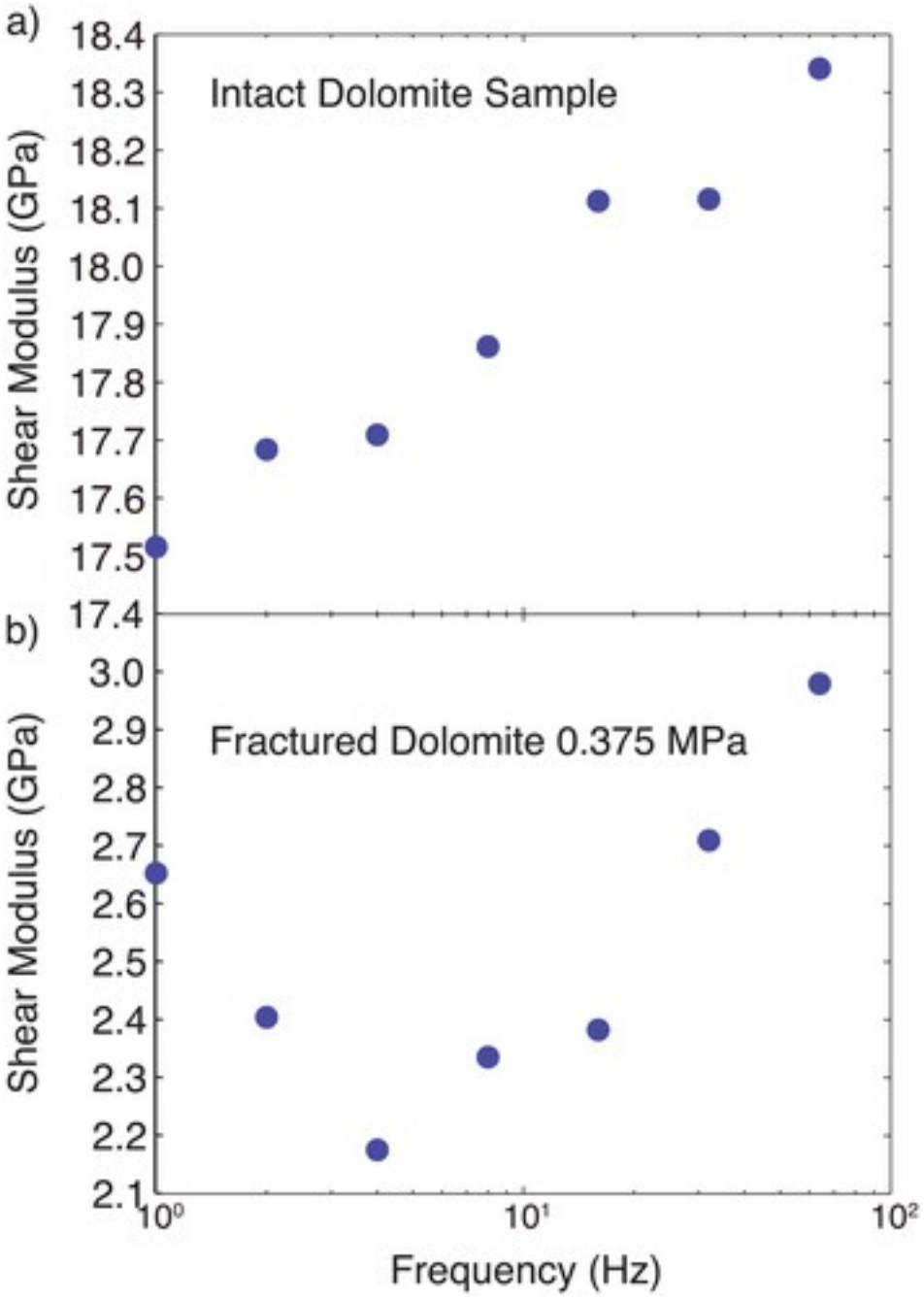

Figure 4

Open in figure viewerPowerPoint

Shear modulus dispersion results for dolomite both (a) intact under no uniaxial load and (b) fractured under 0.375 MPa normal stress with fundamental frequency data. Driving frequency varies from 1 to 64 Hz. The intact sample shows normal dispersion, increasing modulus (or velocity) with frequency (Figure 4a), while the fractured sample shows inverse dispersion at frequencies below about 8 Hz and normal dispersion above about 8 Hz (Figure 4b). This is similar to the frequency dependence of the hysteresis loops explained below, suggesting a low-frequency stiffening mechanism that seems to disappear above 8 Hz.

3.2 Time Series Data: Nonlinear Hysteresis Loops

In addition to using the Fourier transform to isolate the response at the driving frequency, we analyze the time series data of the stress and strain oscillations (Figure 5). Graphing the stress and strain against each other over time provides the stress-strain hysteresis loop, plotted in the inset of Figure 5. If the stress and strain were perfectly periodic, with the strain phase delayed by the attenuation as expected in linear anelasticity, then the hysteresis loop would be an ellipse (periodic fits shown with black lines in Figure 5). Without phase delay the stress-strain curve would be a straight line with the slope given by the modulus, but because the strain follows the stress, the curve starts above this line and returns below the line, creating an ellipse. Throughout the oscillation, the strain rate is also oscillating, so changes in the response due to rate dependence would cause further structure, steepening, or becoming shallower (and their associated changes in modulus) with the changing strain rate.

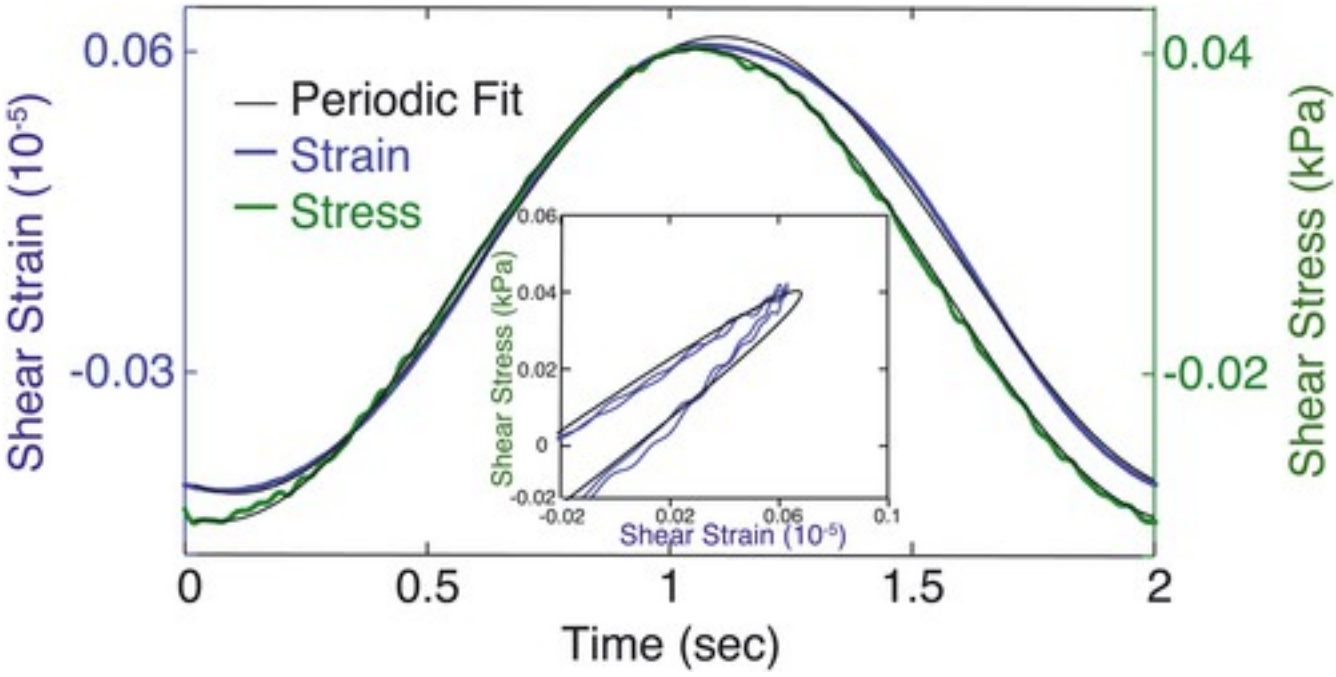

Figure 5
Open in figure viewerPowerPoint
Stress (green) and strain (blue) time series for the Duperow dolomite fracture under 0.375 MPa normal stress and forced with a 0.5 Hz driving frequency. The periodic fit, captured in the fundamental mode data, is plotted in black. The inset shows the stress-strain hysteresis loop, when stress and strain are plotted against each other over time. The data are to first-order periodic but shows further structure provided by the harmonics that are generated by nonlinearities and rate dependence. The high-frequency fluctuations are mainly due to 60 Hz electronic noise.

The stress-strain curve for the intact dolomite without uniaxial load exhibits much less hysteresis and appears linear at the scale of our measurements (Figure 6a), likewise the stress and strain spectra show no clear harmonic generation (Figure 6b). Although we do expect some strain-dependent softening and hysteresis due to attenuation for the microcracked rock, it is much smaller and not visible on the scale of these time series measurements. The intact rock also does not show any strain rate-dependent effects, allowing us to assume that the observed behavior in the fractured rock is due primarily to the fracture and not the intact part of the sample.

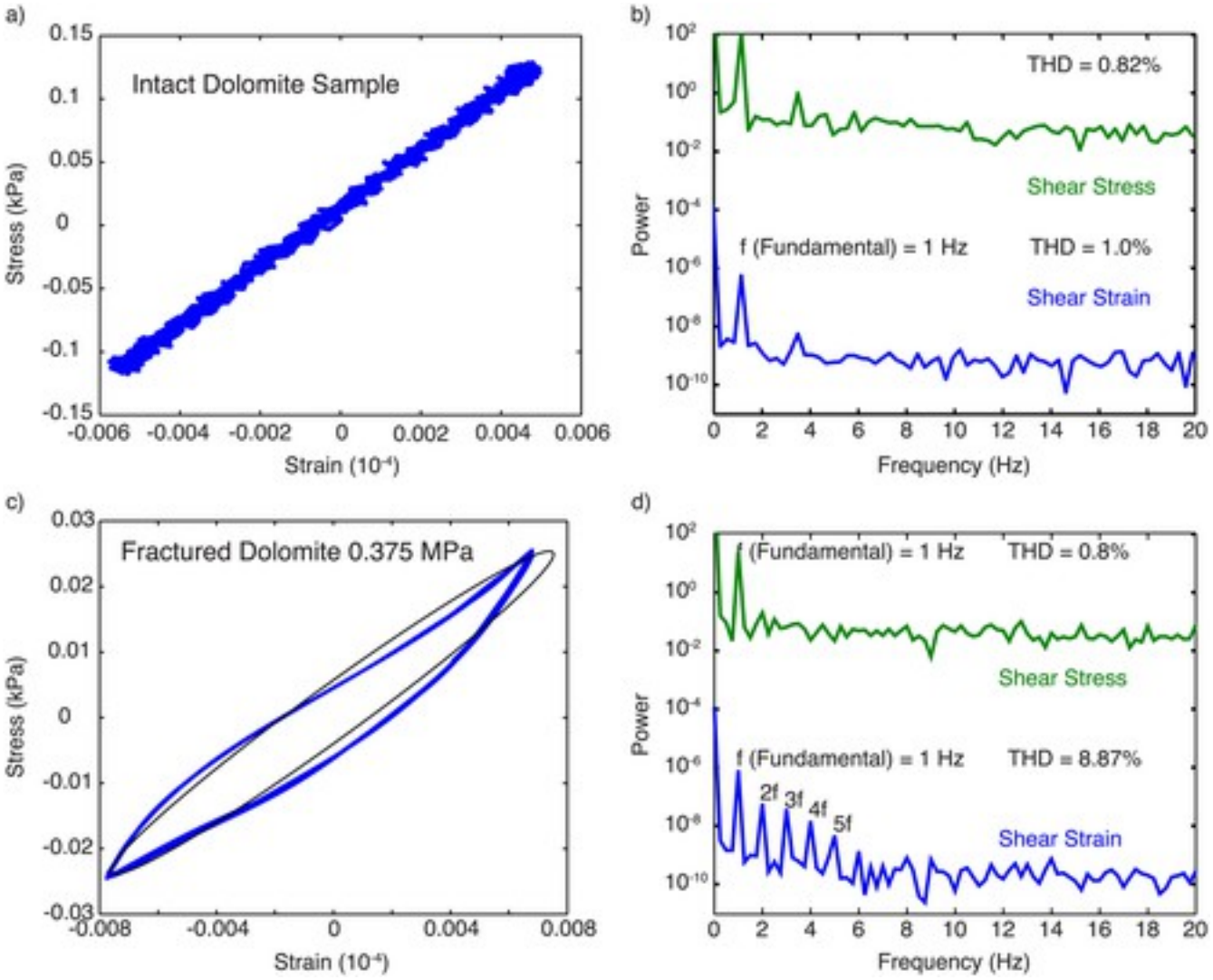

Figure 6

Open in figure viewerPowerPoint

(a) Measured stress-strain loop, in blue, of intact dolomite sample under no uniaxial stress with 1 Hz driving frequency shows no nonlinearity, cusp, or hysteresis. (b) The frequency spectrum also shows almost no harmonic generation; the smaller visible peaks are noise and do not coincide with harmonic frequencies. (c) While the stress-strain loop, in blue, when the dolomite sample is fractured under 0.375 MPa normal stress shows nonlinear hysteresis. The fundamental

frequency data, only including the phase delay between stress and strain, would be the black ellipse, predicted by linear anelasticity. (d) The fractured dolomite's frequency spectrum shows large harmonic generation in the strain, while the stress stays linear. The odd harmonics are slightly enhanced relative to the expected power law decay. This harmonic generation is associated with the nonlinear hysteresis shape and sideband production.

To best visualize the nonlinear hysteresis shape, we low-pass filter to remove high-frequency noise, which is dominated by 60 Hz power noise. This filtered stress-strain hysteresis loop for the fractured dolomite is graphed in blue in Figure 6c. We find that a nonlinear hysteresis shape in the stress-strain loops is accompanied by large harmonic generation (Figure 6d). The added structure in the shape appears most clearly as curled up (stiffening) cusps at the ends of the loop, the stress, and strain sinusoid peaks. These cusps are different from those observed in intact, microcracked rocks at higher strain levels [*Gordon and Davis*, 1968; *McKavanagh and Stacey*, 1974] because they curl up as well as sharpen to a point at the end. For this reason we refer to them as “stiffening cusps.” Hysteresis loops with stiffening at the high strain end have been observed in intact, microcracked rocks under quasi-static uniaxial compression [*Holcomb*, 1981], but the interpretation is different, stiffening is expected due to closure of progressively stiffer cracks with compression. Since our measurements are pure shear, we do not expect a direct strain dependence to cause the observed stiffening; in fact, the direct strain dependence was shown to cause softening (Figure 3c).

The hysteretic loop for linear elastic materials without harmonic generation caused purely by phase delay is an ellipse (graphed in black on Figure 6c), and the area inside the loop is a measure of the energy dissipation or attenuation. The cusped shape comes from harmonic generation in the strain measurement (Figure 6d) and modifies the classical attenuation caused purely by phase delay. The frequency domain stress signal, graphed in green in Figure 6d, does not have harmonics, demonstrating that the source of the nonlinearity is in the rock fracture and not the electronics or magnetic driver. The relative effect of the harmonics that cause the nonlinear part of the hysteresis is a few percent of the total strain amplitude, a second-order effect to the anelastic behavior of the sample. This nonlinear hysteresis and harmonic generation are symptoms of the nonlinear behavior of the fracture, ways to quantify the nonlinearity; the cause will be discussed below.

3.3 Frequency Dependence and Harmonic Generation

Although the times series and hysteresis loops are the most illuminating of the physical processes occurring at the rock interface, they are challenging to measure in a field setting. Harmonic generation and frequency-dependent behavior are more accessible parameters for field-scale measurement techniques. Another measurable effect of this nonlinearity is the production of

sidebands, using amplitude-modulated driving waveforms. When two waves of different frequencies are summed they do not include the sum and difference of these frequencies, or sidebands. In other words, a frequency space representation of this signal will not have peaks at these sum and difference frequencies. However, if this signal is sent through a nonlinear function, the rock in this case, then the sidebands are produced. Thus, measuring sideband production is another metric for nonlinearity and is related to nonlinear wave mixing phenomena [e.g., *Johnson and Shankland*, 1989; *Meegan et al.*, 1993; *Lawrence et al.*, 2008; *D'Angelo et al.*, 2008] and harmonic generation. We measure the harmonic generation with the total harmonic distortion (THD %) [*Ramirez*, 1985], defined as the square root of the power of the first four harmonics over the square root of the power in the fundamental mode. By quantifying the harmonic generation that determines the stiffening cusp shape and the amount of wave mixing with this degree of nonlinearity, we can interpret nonlinear signals from the field for the physical processes and properties discovered in the more complete data available through lab measurements.

We found the stiffening at the static end of sinusoidal oscillations at all low measured frequencies (0.1–6 Hz) (Figure 7a). The cusping effect and harmonic generation diminish at frequencies greater than or equal to about 8 Hz, a threshold frequency (Figure 7b). The stiffening at the cusp is quantified in blue crosses in Figure 7b as the percentage difference in the maximum measured strain and the maximum strain of a periodic fit (at the fundamental frequency) to the data. Also graphed in Figure 7b, in green circles, is the total harmonic distortion (THD %) from the first four harmonics, which shows similar frequency dependence. The fact that the stiffening occurs below an equivalent frequency threshold to the change in dispersion described above (Figure 4b) suggests that they may be due to the same frequency-dependent mechanism. Although the dispersion data in Figure 4b only includes the fundamental mode, it could be that the low-frequency cusp behavior causes a higher measured modulus when present, and thus is responsible for the inverse dispersion below the threshold frequency. This is similar to findings of frictional strength decreasing with frequency below a critical frequency [*Savage and Marone*, 2007].

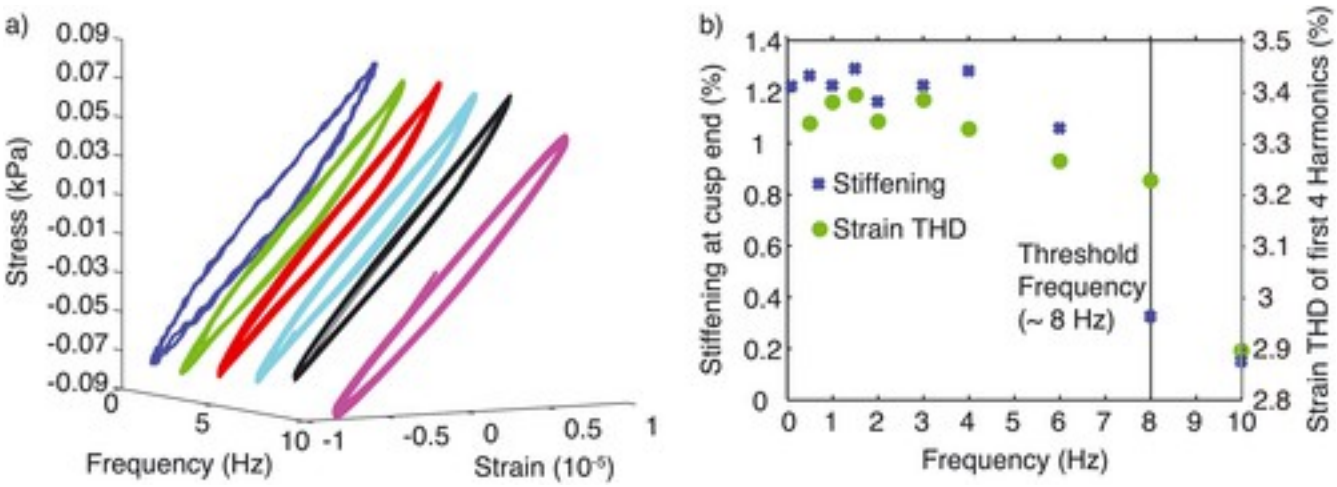

Figure 7

Open in figure viewerPowerPoint

(a) Stress-strain hysteresis loops show stiffening cusps at low frequencies, into the page, but not at 10 Hz, in front. (b) The stiffening (% of periodic fit strain), in blue, and strain total harmonic distortion (THD %), in green, drop around the threshold frequency, ~8 Hz, close to the frequency when dispersion switches in the fundamental data shown in Figure 4b.

As was shown in Figures 6 and 7 above, the harmonic generation occurs under the same conditions as the stiffening cusp shape in the stress-strain hysteresis loop. In fact, the shape is caused by the relative power in these harmonics. They are the same observation; harmonic distortion shows in frequency space what the hysteresis shape shows in time space. Quantitative interpretation of the harmonic signature is outside of the scope of this study, but we note that Figure 6b shows enhanced odd harmonics relative to the expected even harmonics from power law decay. The odd harmonics have a symmetric effect on the hysteresis shape, while even harmonics are not symmetric, so the enhanced odd harmonics are consistent with the predominantly symmetric hysteresis shape. This has been observed in rock, indicating a hysteretic origin [e.g., *Guyer et al.*, 1997].

3.4 Related Rock Fracture Results

Montello granite and Blue Canyon Dome rhyolite were also investigated to evaluate which parts of these behaviors are general and what varies with the rock type and fracture surface geometry. Each of these rocks represents a fractured reservoir or fault of interest, described in methods and materials sections above. The qualitative behaviors of the stress-strain hysteresis shape and harmonic generation, the focus of this study, were observed in all the samples at their lowest measurable normal stresses (Figure 8), suggesting that these kinds of measurements could be used in a range of rock types. We did observe quantitative differences, for example, in the threshold frequency under which the behavior is observed. Past studies have shown qualitatively different frictional behavior for dolomite samples [*Weeks and Tullis*, 1985], which will impact

the parameterization of the data, but the general behavior is still observed in all of our measured samples under these conditions.

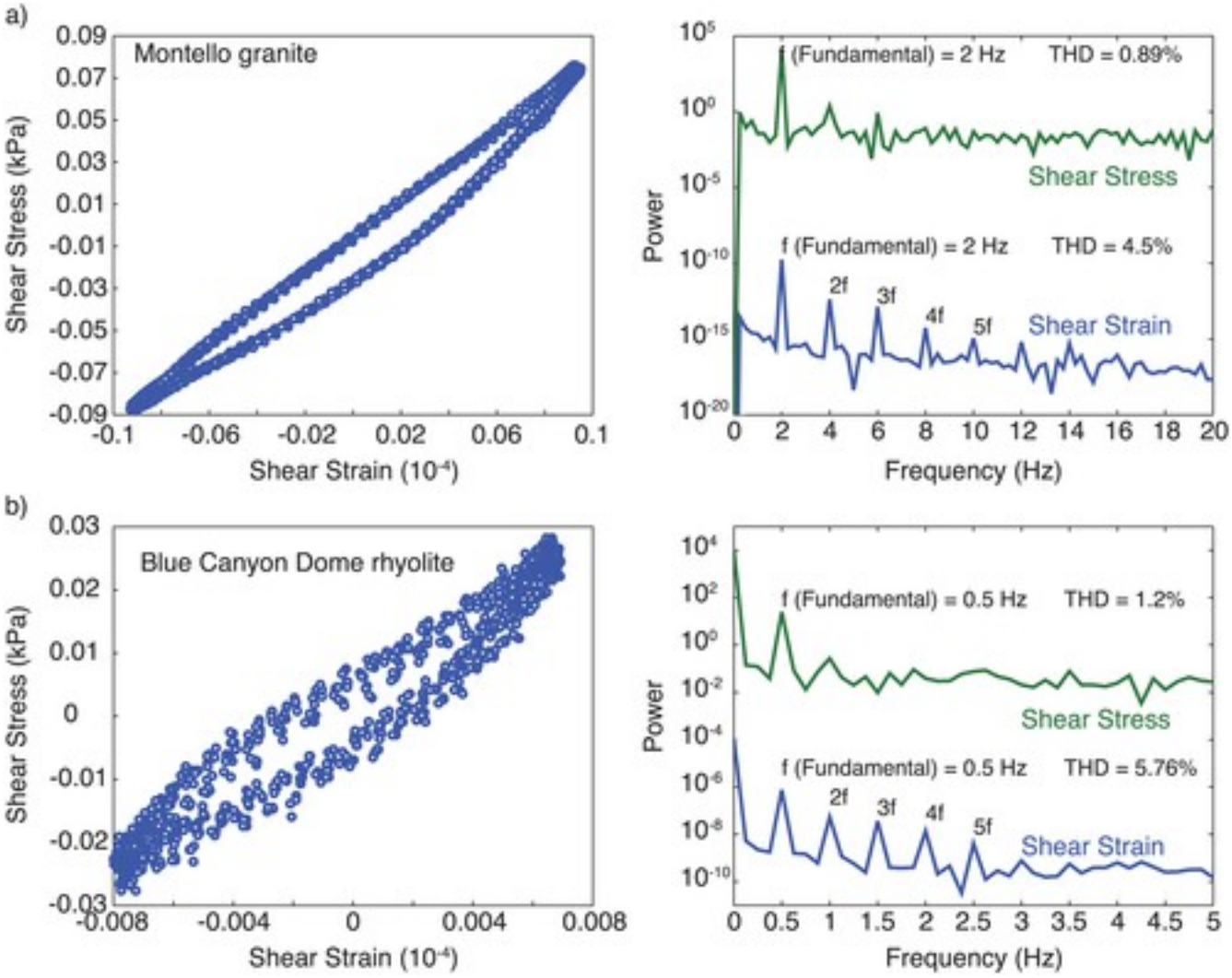

Figure 8

Open in figure viewerPowerPoint

Stress-strain hysteresis loops show similar stiffening cusp behavior for (a) Montello granite and (b) Blue Canyon Dome rhyolite. They both also show harmonic generation in the strain but not in the stress.

4 Discussion

4.1 Mechanism: Dynamic to Static Friction Transition

A past study [*Saltiel et al.*, 2017b] used a simple partial slip friction model to fit our fundamental frequency observations of strain-dependent softening with nonlinear constitutive relations

(Figure 3c), but since this type of friction model has no time dependence it cannot explain the rate-dependent observations of our time series and harmonic generation measurements.

Our hypothesized mechanism comes directly from the time series measurements of strain (Figure 9a). As the strain rate oscillates throughout the sinusoidal forcing, the slipping parts of the fracture surface are expected to transition in frictional value related to the rate-dependent friction value of a dynamic friction model. This can be idealized as, and dominated by, transitioning from dynamic to static friction at the zero strain rate static ends of the sinusoid. The transition to static friction would cause an increase in measured modulus, seen as the bent up cusp at the static end of the stress-strain curve. As the strain rate increases, partial slip renucleates, and the frictional strength of the fracture drops due to the lower value of dynamic friction. This hypothesized mechanism also fits with the observed frequency threshold, where the fracture surface needs to spend sufficient time at low strain rate for static friction to have an effect.

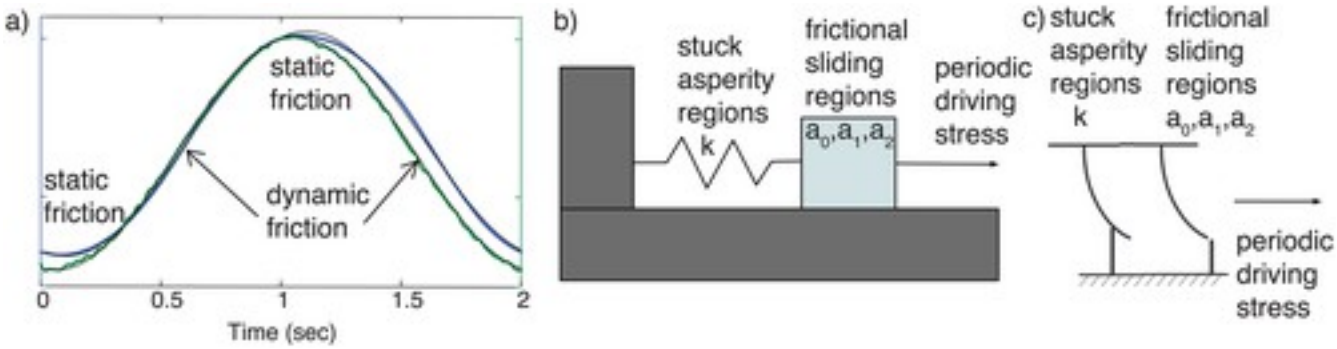

Figure 9

Open in figure viewerPowerPoint

(a) Time series data show the oscillations in strain rate that cause transitions between static and dynamic friction. (b) The slider-block model of the force balance. The periodic driving stress is mostly balanced by a spring representing the stuck centers of the asperities. The spring pulls back on the slider block, which parameterizes the frictionally sliding asperity exteriors. (c) Our model can also be conceptualized as two effective bristles, a commonly used analogy for the Dahl model we implement. The stuck regions are represented by bristles that stay elastic; while the slipping areas are represented by bristles that deform elastically at the static ends of the oscillation, and slide when the strain rate s are high enough.

These measurements take place under partial slip conditions, where regions of the surface asperities are stuck and behave like a linear anelastic material. As the time series data (Figure 9a) show, the strain response is dominated by a phase-delayed periodic signal, so the frictional effects on the measured strain are of second order. It is also clear that the loops are closed, returning to the same initial conditions and not drifting over time, even though the stress has an offset, always pushing in the same direction and oscillating the stress on top of this offset. This

means that the displacement is growing and shrinking but always positive, while the velocity is negative half of the time. For this reason, the stuck regions must be included in the force balance to provide the restoring force that pulls back the slipping regions.

A simple slider-block model best illustrates the force balance, where each component of the system response is represented by an element that has its own parameterization in the equation. To accommodate the stuck asperities, we include a spring holding back the slider block and held fixed on the farside, as shown in Figure 9b. The spring supplies a restoring force in the form of Hooke's law. The slider block represents the frictional resistance on the slipping sections of interface asperities. A dynamic friction model parameterization, described below, is implemented on the block to capture the changes in friction we observe. The slider block is forced with a periodic stressing, which is balanced, mostly, by the spring, representing the stuck asperities, and to second order by friction on the slider block. We model the behavior using a single block and spring, but these elements each represent many locked and sliding regions. This force balance is expressed in the following equation:

$$\gamma F_d = kx + F_f(v, \theta, \text{model parameters}) \quad (1)$$

where γ is a stress concentration factor that scales the bulk shear stress to the shear stress felt by the smaller area asperities; F_d is the periodic driving force, which is converted from our stress data; k is the spring constant that represents the stuck asperities; x is the displacement of the block, which we will be solving for; and F_f is the friction force on the block, a function of slip velocity, v, a state variable, θ, both of which evolve over time, and other model parameters. We use a modified Dahl friction formulation, described below, to solve for the friction force on the sliding block.

The model makes a few key assumptions and simplifications to distill the dynamic frictional behavior of interest. First, the inertial term is dropped, because acceleration is assumed small. This is a reasonable assumption since we are using subresonant frequencies. It is inertia that causes resonance; since we are driving the system at low frequencies, the acceleration of the block is negligible. This is the same assumption that is made for all subresonance measurements, equivalent to saying that the stress is transmitted evenly across the sample [*Saltiel et al.*, 2017a]. Next, the model is designed for linear slip geometry, while we are slipping in torsion, but each of the asperities individually are deforming linearly in the tangential direction, given our small angular displacements. Although each asperity is experiencing a different forcing depending on its placement on the fracture surface, as shear stress and strain scale with radius and interaction with neighboring asperities, these effects are not directly addressed, contributing to the effective nature of parameters in the model fit. The only place in the model that treats the size of asperities is the stress concentration factor, γ, which should depend on the real contact area that stresses are transferred through compared to the total cross-sectional area over which we calculate the bulk

stress. The pressure-sensitive film measurements give an estimate of the normal stress concentration factor of ~80, where we resolve ~40 MPa normal stresses on individual asperities when the entire fracture is under 0.5 MPa normal stress (Figure 2d). The model fit, described below, requires a stress concentration factor of ~72, consistent with the estimate provided by the pressure sensitive film.

4.2 Modified Dahl Model: Bristle Analogy

Rate-dependent frictional behavior observed in fault friction community from velocity-step experiments is commonly parameterized with the rate-and-state friction model [*Dieterich*, 1979; *Ruina*, 1983]. This model has also been analyzed using stability theory, predicting the boundary between steady sliding and unstable stick slip based on the rheological critical stiffness [*Gu et al.*, 1984]. However, the rate-and-state formulation is unable to capture static friction or reverse slip because it is numerically unstable at zero or negative slip velocities [*Dieterich*, 1979; *Ruina*, 1983]. Rate and state uses a logarithm of velocity dependence ($F_f \sim \log(v/v_0)$), which means that solving for negative velocities is not possible. Other fault friction models, such as the Brittle-Ductile friction model [*Trugman et al.*, 2013], use a slightly different formulation ($F_f \sim \log(v - v_0/v_0)$), but they still are not symmetric about zero velocity, even giving the frictional force in the wrong direction for reverse slip. Thus, a different velocity dependence formulation is necessary to model slip velocity reversals and the effect of static friction.

Other friction models, such as in *Dahl* [1976], have been formulated by the control and dynamics engineering communities to capture reverse slip and zero velocity crossings [*Pennestrì et al.*, 2016; *Péter et al.*, 2014]. The observation of increased static friction at zero velocity is referred to as the Stribeck curve [*Stribeck*, 1902], and these models can be modified to capture this behavior [*Canudas de Wit et al.*, 1993]. While it is not the only suitable formulation, the modified Dahl model captures the zero velocity crossing effects, while retaining a form similar to rate-and-state friction. Although it has six free parameters, it still has fewer parameters than many other models in this class [*Pennestrì et al.*, 2016]. From our literature search, we found the modified Dahl model to be the simplest model that retains the hypothesized physical processes and whose parameters have some physical interpretation [*Péter et al.*, 2014]. For these reasons, we explore the Dahl friction parameters that would create our observed strain rate-dependent hysteretic stress-strain loops. The focus here is to test whether this model can match the observations, providing support for the hypothesized mechanism and a potential path forward for analyzing the frictional signature in this type of data.

As the Dahl friction formulation is not commonly utilized by the Earth science literature we describe a little of its physical basis. The Dahl model is in the class of “bristle” friction models. These models describe the onset of frictional sliding as the initial elastic deformation and subsequent permanent displacement of a bristle, such as on a brush. This analogy is also useful in describing partial slip. A bristle that never reaches slipping conditions could describe the stuck regions of the asperities, in place of the spring. Our force balance, Figure 9b and equation 1, could be illustrated with two different bristles in series, one of which never slips, equivalent to the spring, while the other sticks at low velocities than slides frictionally above a characteristic velocity, v_s, captured in the slider block's frictional parameterization (Figure 9c). This characteristic velocity defines the velocity range over which the higher static friction value is applied. The model includes these essential features—a continuous function around zero velocity, which is numerically stable, and velocity dependence that fits the Stribeck curve, which shows higher friction values at low velocities representing the effect of static friction. The modified Dahl model [*Canudas de Wit et al.*, 1993] is given in the following equations:

$$F_f = a_2 \frac{v}{v_0} + \theta \quad (2)$$

where a_2 is the viscous friction parameter, because it gives the proportionality between the friction force and velocity. The state variable (θ), with units of force, evolves based on the following equation:

$$\frac{d\theta}{dt} = \frac{-\mathrm{abs}[v]\theta}{L} + a_0 \frac{v}{L} + a_1 \frac{v}{L} e^{-\left(\frac{v}{v_s}\right)^2} \quad (3)$$

where L is a constant with dimensions of length related to the critical slip distance; v_s is the characteristic (Stribeck) velocity, described above; a_0 is the Coulomb friction parameter; and a_1 is the Stribeck friction parameter, defining the weight of the static friction effect.

4.3 Comparison of Model to Observations

We want to test if the modified Dahl model is able to capture the general nonlinear shape of our observed hysteresis loops at low frequency, with the right choice of parameters. To solve this set of ordinary differential equations 1–3, we use a real-valued variable-coefficient solver, with fixed-leading-coefficient implementation, VODE in the scipy package [*Brown et al.*, 1989]. Since there is a large parameter space, we used the python package S-timator [*Ferrira*, 2016], which implements a differential evolution genetic optimizer [*Storn and Price*, 1997]. To find parameters that match the observations, we allowed all the slider block model parameters, as well as the initial strain and strain rate, to vary. Only the length constant, L, was held fixed to 3×10^{-6} m (similar to estimates of the critical slip distance from *Saltiel et al.*[2017b]). The model was driven with a linearized forcing from the measured stress data (Figure 6a). This was not a

thorough inversion; we focused on confirming the models ability to reproduce the observation using reasonable parameters.

The model results are shown in Figure 10, using the following best fit parameter values: $a_0 = 2.9 \times 10^{-6}$ N, $a_1 = 16$ N, $a_2 = 2$ N, $\gamma = 72$, $k = 4.5 \times 10^{6}$ N/m, $v_s = 7.3 \times 10^{-8}$ m/s, and $v_0 = 1.3 \times 10^{-5}$ m/s. Figure 10a shows the direct comparison between the modeled and observed stress-strain hysteresis loops. The modeled stress and strain oscillations are shown in Figure 10c, and the frequency spectrum are shown in Figure 10d. The model is not able to fit both the middle of the oscillation and the cusped ends with the same set of parameters. The key to fitting the cusped part of the data was to fit the strain rate, not the strain, from the data, effectively weighting the ends over the other parts of the sinusoid. The model results mimic the symmetric part of the stiffening shape, resulting only from odd harmonic generation, but cannot generate even harmonics. This suggests that the even harmonics in the observations are due to higher-order, nonsymmetric, physical mechanism, not captured by this model. A possible nonsymmetric mechanism, not included in the model, is the direct strain-dependent softening (Figure 3c). This softening could cause the lower stress values in the center of the experimental hysteresis loop, compared to that from the model, fully symmetric, results (Figure 10a). The slightly less defined stiffening at the low strain static end compared to the high strain end (Figure 10a) could also be effect of direct strain-dependent softening. A model that also captured this direct strain dependence should generate even harmonics and better fit the observations.

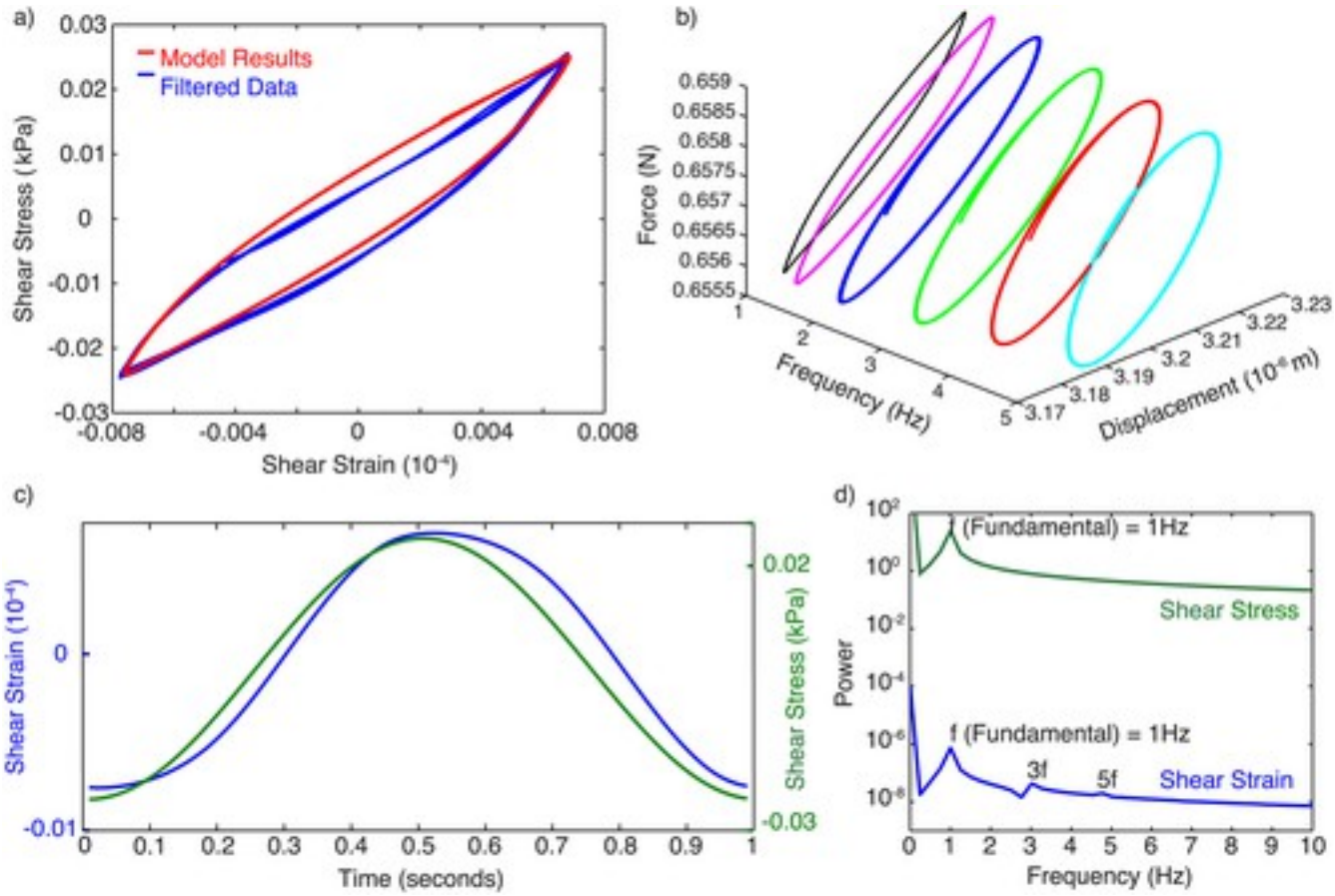

Figure 10

[Open in figure viewerPowerPoint]

The model results with the best fit parameters given in text. (a) Stress-strain hysteresis loop from model (red) compared to our data (blue). (b) Modeled hysteresis loop shapes show a continuous decrease of cusp shape and increase of phase delay with frequency. (c) The model predicted time series of strain (blue) given a periodic driving stress (green) and (d) the frequency space representations. The strain only exhibits odd harmonic generation, while the stress has no harmonics because a periodic forcing is used. The model generates smaller harmonics than the data and only odd harmonics, suggesting that the even harmonics are due to another, nonsymmetric, mechanism.

Both through the physical interpretation of the parameters and numerous forward model runs with varying parameters, we find that a_1 and v_s have the greatest effect on the hysteresis shape, while the balance of the other parameters mostly affects the amplitude, saturation, drift, and damping of the resulting strain. The low value of a_0 suggests the minimal importance of Coulomb friction. The velocities between v_s and v_0 are where we expect to see the effect of static friction. Since the model has many parameters, there are many different regimes of parameter space that show varied behavior. The similarity of the results suggests that the model is able to capture the basic processes in our experiments at these conditions.

To better understand the model behavior, we focus on this set of parameters that best fit our data but with different forcing frequencies. The modified Dahl model results also show frequency dependence (Figure 10b), but the high-frequency behavior is different from our experimental results. Instead of exhibiting a threshold frequency, around 8 Hz for the dolomite fracture, the hysteresis loop undergoes a more gradual change in shape with frequency, and it begins at slightly lower frequencies, ~2 Hz, than the data. The stiffening cusp diminishes with frequency as the measurements show, but it is accompanied by a growing phase delay, which is not present in our experimental data. These effects are clear in the high-frequency large ellipses (Figure 10b), which eventually grow to circles, phase delay of 45°, at even higher frequencies, not shown. Finding the fitting parameters for the data at each frequency independently could show the frequency dependence of each parameter. Another possibility is that a more complicated model could better capture our experimental high-frequency behavior. Higher driving frequencies cause higher slip velocities, greater than v_0, so a compound model with a rate-and-state friction formulation above v_0 and the modified Dahl model for lower slip velocities, at the static friction condition, would change this high-frequency behavior. Future work will explore model variations and their parameter regimes, employing stability theory to understand the transitions between regimes and their dependence on the balance of model parameters. Better understanding of the behavior of the many model parameters will allow consistent data parameterization, quantifying the dynamic friction signature of lab and, eventually, field data. To do this properly may also require accounting for the complex surface and asperity geometry.

5 Conclusions

We present seismic-frequency torsional oscillation measurements of stress and strain on rock fractures under low normal stresses, conditions that have been shown to produce partial slip on the outside of asperities while the centers remain stuck and elastic. Our results suggest the signature of dynamic friction, variations in friction or stiffness as strain rate oscillates during the periodic driving stress. This process is most apparent in our measured strain time series compared to a periodic fit. The largest deviation from the fit is when the strain falls short of reaching the expected peak at the static end where strain rate goes through zero. The dominant frictional effect is due to static friction at this static end transitioning to and from dynamic friction in the higher strain rate parts of the cycle. The stress-strain hysteretic loop shape expresses this effect with stiffening cusps at the static ends. This nonlinear hysteresis is accompanied by harmonic generation in the strain, while the stress remains linear, confirming that the driver and electronics are not the source of the nonlinearity. Lastly, the observed

frequency dependence also supports this mechanism. We see stiffening cusps, harmonic generation, and modulus decreases with frequency at low frequencies (< 8 Hz), while the higher frequencies retain more linear hysteresis shapes, lower harmonic generation, and normal dispersion. We interpret that this shows longer periods, lower frequencies, that are needed to spend sufficient healing time at low strain rates for the static friction to have an effect. Otherwise, at high frequency, the slipping parts of the fracture keep slipping and the fracture lacks the added nonlinear hysteresis and stiffening. Since low-frequency apparatuses are rare, especially for measuring fractures under low normal stress, these results suggest that there may be physical processes that are being missed by higher-frequency experiments.

Taking advantage of model development in the dynamics and control engineering communities, we adapt a modified Dahl model to capture the described mechanism and show the parameters necessary for the observed behavior. This “bristle” model, coupled to a spring describing the stuck parts of the asperities, is able to show the effect of higher static friction as strain rate is reversed through zero, known as the Stribeck effect. Although not unique given the large number of parameters, the Dahl model produces qualitatively similar strain oscillations and hysteresis loops, given a periodic driving stress. The Dahl model is also attractive because it has a similar functional form to rate-and-state friction, allowing data parameterizations to be compared to rate-and-state friction parameters commonly used to describe fault and earthquake nucleation behavior. The rate-and-state friction model itself cannot be applied to these measurements because it is unable to model zero velocity or velocity reversals. More work on models that include both formulations and stability analysis is needed to parameterize data in a way that allows field measurement of dynamic friction properties.

These results provide a path for using high-amplitude, active source seismic methods, such as provided by time reversal techniques, to probe frictional properties in reservoir fractures and faults in the field. There are also implications for the characterization and underlying physical processes of bulk nonlinear elasticity in Earth materials, suggesting that fast and slow dynamics are related to dynamic frictional effects such as aging and healing. Although it will be challenging to measure stress-strain time series or hysteresis loops in the field, the accompanying harmonic and sideband generation could be measurable with repeatable crosswell surveys where strains in the 10^{-5} range can be achieved with appropriate high energy sources. The fact that the frequency dependence occurs in the seismic frequency band suggests that these effects could be measured directly in the field. Such an approach could potentially provide spatially resolved constraints on the frictional behavior (such as velocity strengthening or weakening properties) of critically stressed faults in the absence of seismicity.

Acknowledgments

This research was funded as part of the Big Sky Carbon Sequestration Partnership (BSCSP) by the U.S. Department of Energy and the National Energy Technology Laboratory through award number DE-FC26-05NT42587. The Big Sky Carbon Sequestration Partnership – Phase III quarterly progress report [*Spangler*, 2014] is on file at Montana State University, P.O. Box 172465, Bozeman, MT 59717-2465, and is available to the public by sending an e-mail request to bigskycarbon@montana.edu. Secondary support for J. Ajo-Franklin was provided by the U.S. Department of Energy, Office of Science, Office of Basic Energy Sciences, Chemical Sciences, Geosciences, and Biosciences Division under contract DE-AC02-05CH11231. We would like to thank Lee Spangler and the BSCSP leadership for access to the Duperow dolomite sample. We would like to thank Hunter Knox and Mark Grubelich (Sandia National Laboratory) for access to the Blue Canyon Dome rhyolite sample. We would also like to thank Paul Selvadurai, Seiji Nakagawa, and Bruce Buffett for useful suggestions and assistance in sample characterization. The experimental data for this paper are available by contacting Seth Saltiel at ssaltiel@lbl.gov.